Journal of Civil Structural Health Monitoring (2022) 12:391–409
https://doi.org/10.1007/s13349-022-00549-5

ORIGINAL PAPER

Experimental vibration analysis of large structures using 3D DIC technique with a novel calibration method

David Kumar[1] · Chih-Hung Chiang[1] · Yung-Chiang Lin[2]

Received: 31 May 2021 / Revised: 1 October 2021 / Accepted: 6 January 2022 / Published online: 25 January 2022

Abstract
A novel calibration method is developed for calibrating stereo-camera-based digital image correlation (DIC) setup to overcome the difficult challenge of 3D vibration measurement of large structures using digital imaging techniques. The calibration method employs an IMU sensor for camera orientations, a laser sensor for camera positions, and a virtual stereovision approach for intrinsic parameters. This novel stereo-camera calibration method is validated using an ideal physical calibration method and then integrated with DIC technique for field experiments. The first field experiment is performed on a light tower of 10m height. The results showed that the developed technique can measure 3D displacements of the light tower under various excitation modes. It was also consistent in terms of natural frequency estimation which is validated using an accelerometer. With this success, the developed methodology is employed in the second field experiment where 3D vibration study is carried out on a utility-scale wind turbine. The developed DIC-calibration method is able to obtain the in-plane and out-of-plane displacements of the tower and rotor blade of the turbine. The method is also able to produce accurate values of natural frequencies validated using a ground-based microwave interferometer. It can be said that the present study established a stereo-camera-based DIC technique with a novel calibration method for 3D vibration analysis of various large-sized civil and aerospace structures.

Keywords Digital image correlation · Nondestructive testing methods · 3D vibrations · Structural health monitoring · Large structures · Stereovision calibration

1 Introduction

Structural health monitoring of large-sized civil structures using digital image correlation (DIC) methods has made a significant progress [1–3]. However, there are challenges that need to be addressed, particularly in the case of wind turbine towers and blades. These structures generate in-plane and out-of-plane deflections as well as 3D vibrations during their operation cycles. Wind turbines are constantly under the influence of lightning, wind gust and even earthquakes that can lead to severe damage on the supporting tower and the rotor blades [4]. Therefore, studying vibrational characteristics is useful to asses a structure's condition and identify damage as well as for the future design and analyses [5–7]. The present study is based on advancing DIC techniques by developing a suitable stereo-camera calibration method to perform experimental 3D vibrations studies of large-sized structures for the health monitoring purposes.

DIC technique is a non-contact technique which can be used for measuring 2D–3D displacements and strains of various materials and structures [8, 9]. Peters and Ranson [10] introduced this technique in 1982. Sutton et al. [11] extended this technique and developed numerical algorithms to perform image correlation over optically recorded images. The authors developed improved DIC methods and used them to measure full-field in-plane deformations (2D-DIC). In 1992, Luo et al. [12] extended 2D-DIC to 3D-DIC using

✉ Chih-Hung Chiang
chiangc@cyut.edu.tw

David Kumar
davidcyut@cyut.edu.tw

Yung-Chiang Lin
yclin1977@cyut.edu.tw

[1] Department of Aeronautical Engineering and Center for NDT, Chaoyang University of Technology, Taichung 413310, Taiwan

[2] Department of Construction Engineering and Center for NDT, Chaoyang University of Technology, Taichung 413310, Taiwan

pinhole and stereovision camera models. Silva et al. [13] and Orteu [14] also worked on the development of 3D-DIC and stereo camera calibration methods. Reu published a series of articles under the title of The Art and Application of DIC that are very useful for developing DIC setups for laboratory as well as field experiments [15]. Considering its applicability, DIC technique can be used for various time and length scales [16]. There is significant work carried out on high-speed DIC as well as application of DIC for deformation measurement on small-size scale materials and structures. In another study, we developed a novel in-house high-speed 3D-DIC technique for motion measurement of light and flexible structures [17]. Recently, many researchers have started using DIC technique for displacement measurement and vibration studies of large structures such as wind turbines and bridges. However, most of the studies are based on the application of single camera DIC which is useful to measure in-plane displacements [18–23]. Wang et al. [24] obtained vibrational parameters of a high guyed mast telecom structure using a smartphone camera. The authors performed correlation-based template matching on the images extracted from the smartphone videos of the components of the guyed mast, i.e., guy cables, cable anchor and antenna. Brown et al. [25] used a video- and laser-based sensing technique to measure in-plane displacements and rotations of various civil structures. The technique uses a camera mounted on the moving subject which tracks light dots from two laser emitters placed off-structure at a fixed station. The study adopted various computer vision tools such as cross-correlation, distortion correction and camera calibration that are available in MATLAB. The authors reported that up-sampled cross-correlation technique (also known as single-step DFT) is more accurate than traditional cross-correlation and centroid detection techniques. In our previous study, single camera DIC was used for measuring in-plane displacements of a highway bridge, which was validated using LVDT [18]. Efforts are being made to apply two or more camera-based DIC for 3D displacement measurements of large structures [26–28]. However, there are still challenges remain in the accurate measurement of 3D displacements and vibrational parameters of large-sized civil structures. In addition to these challenges, another key difficulty in testing large structures using DIC is the calibration of the stereo-cameras. In another study [29], we developed a 3D-DIC setup, which was successful in the measurement of in-plane and out-of-plane displacements validated using a micrometer and a Vernier caliper, respectively. However, the method was not successful in the field experiments due to the limitation of using indoor-scale stereo-DIC calibration method that uses a physical calibration board. Hence, a suitable calibration technique has to be employed for accurate estimation of intrinsic and extrinsic parameters of the stereo-DIC system in the field. Sabato et al. [30–32] have developed an IMU-radar sensor board for 3D-DIC calibration. This is very useful technique for the measurement of extrinsic parameters for large structures. Also useful in the case of moving cameras as seen in unmanned air vehicle (UAV) assisted health monitoring [33–36]. In an earlier study [37], we reported that this calibration method could be enhanced by an intrinsic parameters measurement approach.

In the present study, a novel calibration method is devised that uses IMU and laser sensors along with a virtual stereo-vision tool for obtaining extrinsic and intrinsic parameters of a stereo-DIC setup for large structures. The calibration method is integrated with the DIC technique and implemented for estimating 3D vibration parameters of a light tower of 10 m height and a wind turbine of 65 m tower height and 70 m blade diameter. The vibrational parameters such as 3D displacements and natural frequencies have been obtained and studied to demonstrate the capability of the developed methodology.

2 Development of a novel calibration method for large structures

The study explores three-dimensional computer vision-based DIC technique to study vibrational characteristics of large structures. The following sections describe the theoretical background as well as development and validation of a novel calibration method for two-camera-based stereovision system designed for large structures.

2.1 Pinhole and stereovision models for DIC applications

Pinhole projection model relates a point in real world to its projected location in an image. The model basically includes three elementary transformations from world coordinate system to sensor-image coordinate system. The geometry of the pinhole model for a camera is shown in Fig. 1. For a point M in three-dimensions, the coordinates in world coordinate system (denoted by R_w) are (X_W, Y_W, Z_W) . Camera coordinate system is denoted by R_c with center C and coordinates (X, Y, Z). Image plane coordinate system is denoted by R_r with coordinates (x_i, y_i). Sensor-image coordinate system is denoted by R_s which has an image point m with the coordinates as (x_s, y_s). The image point m (measured in pixels) is the image location of M (measured in metric units) from world coordinate system, the mathematical representation can also be seen in Fig. 1. The first transformation defines the relationship between world coordinate system and camera coordinate system. This transformation involves extrinsic parameters such as rotations and translations that relate a camera to the external points in the real world. The second transformation is the projection transformation of camera

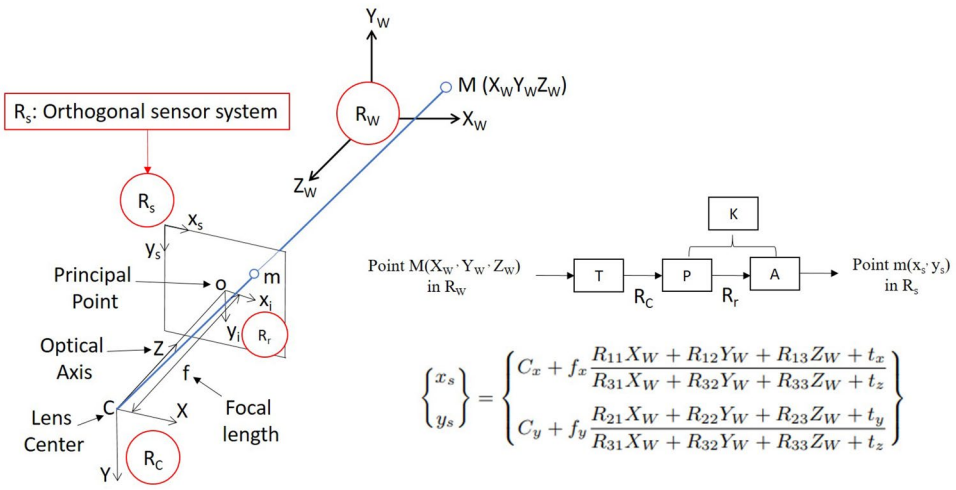

Fig. 1 Description of pinhole model for a camera, where [T] is the rigid body transformation from world coordinate system to camera coordinate system using rotation and translation (matrix of extrinsic parameters), [P] is the perspective projection from camera coordinate system to image plane coordinate system using focal length, [A] is the transformation from image plane system to sensor image system using scale factors (metric to pixel) and principal points, [K] is the matrix of intrinsic parameters combining [P] and [A].

coordinate onto the image plane. The third transformation involves the transformation of the point in image plane to the sensor coordinate system. The second and third transformations use intrinsic parameters such as principal points (c_x, c_y) and focal lengths (f_x, f_y). There are two other type of intrinsic parameters known as skew angle and distortion coefficients. Sometimes, the sensor array/image may be skewed which affects the transformation between image plane and sensor plane systems. In the present study, the sensor-image plane is considered orthogonal by making the use of suitable skew-free digital cameras. An ideal pinhole model considers distortion free images due to which the calibration could be performed using linear transformation models by employing homogeneous form of the transformations. In the presence of distortion effects, the pinhole model can be integrated with nonlinear distortion coefficients forming a nonlinear calibration model. This calibration model can be solved using bundle adjustment technique which is originated from photogrammetry applications.

Three-dimensional digital image correlation (3D-DIC) is based on a stereovision system, and the relation between world and sensor coordinate systems for stereovision system can be obtained using pinhole model by employing it for two cameras set in binocular stereovision configuration. The geometry and mathematical presentation of two-camera stereovision system are shown in Fig. 2. The intrinsic and extrinsic parameters are required for reconstruction from correlated points (x_s^i, y_s^i) present in the cameras (i is 1 for left camera and 2 for right camera) to the corresponding location (X_W, Y_W, Z_W) in the world coordinate system. The intrinsic and extrinsic parameters can be obtained using a stereovision calibration method. The stereovision systems can be calibrated in two ways: (1) stereovision-independent camera calibration, (2) stereovision-combined camera calibration. In the case of the first method, the calibration plate is associated with the reference coordinate system. Whereas, in the

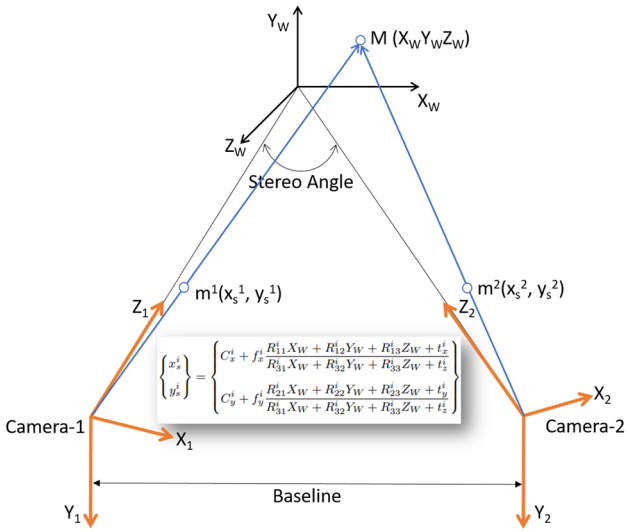

Fig. 2 Stereovision model for 3D-DIC setup, where i is 1 for left camera (also referred as camera-1) and 2 for right camera (also referred as camera-2), (X_W, Y_W, Z_W) are the coordinates in the world coordinate system, (X_1, Y_1, Z_1) are the coordinates in the camera-1 coordinate system, (X_2, Y_2, Z_2) are the coordinates in the camera-2 coordinate system.

second case, one of the cameras is considered as the reference coordinate system. For 3D-DIC applications, the second method, i.e., stereovision-combined calibration model is used for calibration while the reference axis is placed on the left camera. A detailed mathematical background and the working procedures of the camera calibration methods can be found in [13, 14, 38, 39].

2.2 The proposed calibration approach

During a calibration process, a calibration plate is placed in the field of view (FOV) of both cameras. The calibration

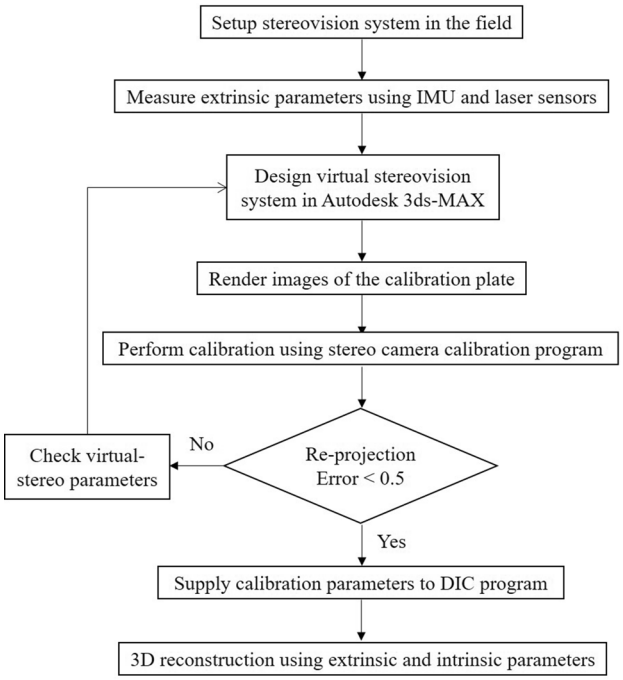

Fig. 3 Flowchart of the calibration methodology

plate is generally designed with unique features/points at known locations (a calibration pattern) required for calibration purpose. The dot-grid and checker-board are the mostly used calibration patterns for camera calibration. The pictures are recorded simultaneously using both of the cameras while the calibration plate is being positioned at different orientations and translations. However, the use of the calibration plate is feasible only for small-size materials and structures. It is extremely challenging and impractical for large structures. This is one of the great challenges in performing DIC experiments for studying large-sized structures. To overcome this everlasting issue, we have developed a novel calibration method which uses physical and virtual tools and eliminates the requirement of a physical calibration board. The proposed calibration approach is described in Fig. 3. This innovative and unique calibration method is explained and validated in the following sections. Finally, it is then applied for calibrating the stereo-DIC setups used in the field experiments.

2.2.1 Extrinsic calibration

In the present study, the extrinsic parameters were obtained using IMU and laser sensors. The IMU sensor provides orientation angles of the cameras, whereas the distance between the cameras and also cameras to the structure were obtained using laser sensors. The IMU sensor used in this study is basically a 9-axis inertial sensor that consists of 3-axis gyroscope, 3-axis accelerometer, and 3-axis magnetometer. This sensor was programmed with Arduino microcontroller (Arduino MEGA R3) to acquire the camera rotation angles. The programming was done using inbuilt programming tool in Arduino software. The IMU sensor can measure orientation angles with an accuracy of less than $\pm 0.1°$. It was validated using mobile application based measurements. The laser sensors were used directly as they are off-the-self instruments which have a validation certificate from the maker. The components of extrinsic calibration setup are shown in Fig. 4.

2.2.2 Stereovision calibration

As it is mentioned before, the intrinsic parameters for a camera are principal points in X and Y axes, focal length in X and Y axes, skew angle, and distortion coefficients. The effect of skew angle is not considered in this study by considering that the used digital camera would provide skew free images. Most of the modern high-end digital cameras such as Sony $\alpha 9$ provide skew free images. Many other studies also shown that the value of skew angle is mostly under 1° [40, 41]. In the present study, the intrinsic parameters were obtained with the help of a virtual stereovision system designed in Autodesk 3ds-MAX. To design a virtual system in the 3ds-MAX, the required parameters are basically camera specifications and the extrinsic parameters. The camera specifications required are focal length of the lens and the physical size of camera sensor. The extrinsic parameters were taken from the IMU and laser sensors. As far as the distortion effects are concerned, they were obtained and corrected separately. At the same time, the experimental images

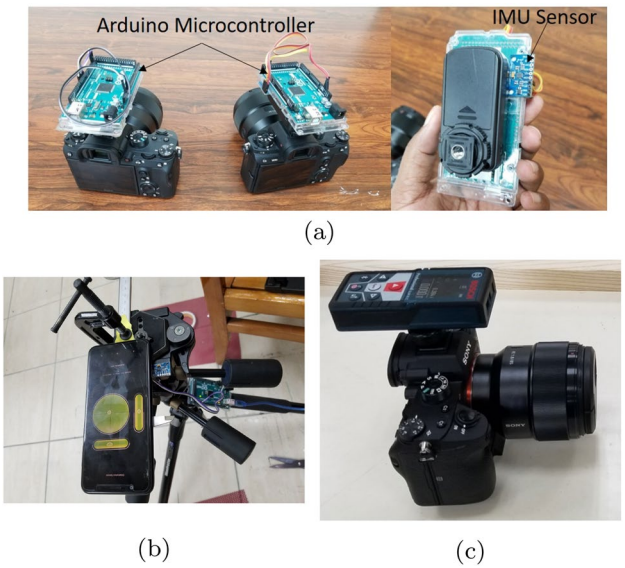

Fig. 4 Extrinsic calibration setup, **a** Cameras with IMU-Arduino device, **b** Validation of IMU measurements using mobile, **c** Camera with laser sensor

were corrected before they were supplied to the DIC program for correlations purposes. The distortion coefficients were obtained by performing individual camera calibration experiments. They can also be rendered from the camera manufacturer. The first-order radial distortion model was applied for correcting the images [42]. A program was developed that takes the recorded experiment images and correct them for distortion. Thus, the contribution of the distortion is removed from experiments as it is not considered in the virtual system. This makes the comparison of physical and virtual system feasible. Figure 5a shows a virtual stereovision system which can be designed in the 3ds-MAX for a particular field experiment. It has two cameras as well as a calibration plate placed in the FOV of the cameras. Checkerboard-based pattern is used on the calibration plate for the calibration process. The calibration plate can be translated and rotated at desired values to render the calibration images. Sample of the various calibration images can be seen in Fig. 5b.

2.2.3 Experimental validation

To validate the calibration methodology developed in the present study, we devised an ideal experimental calibration setup which consists of a warping proof large A0 size calibration board made out of thick foam supported by wooden frame on the sides. This experimental calibration setup is shown in Fig. 6. In this setup, the calibration board

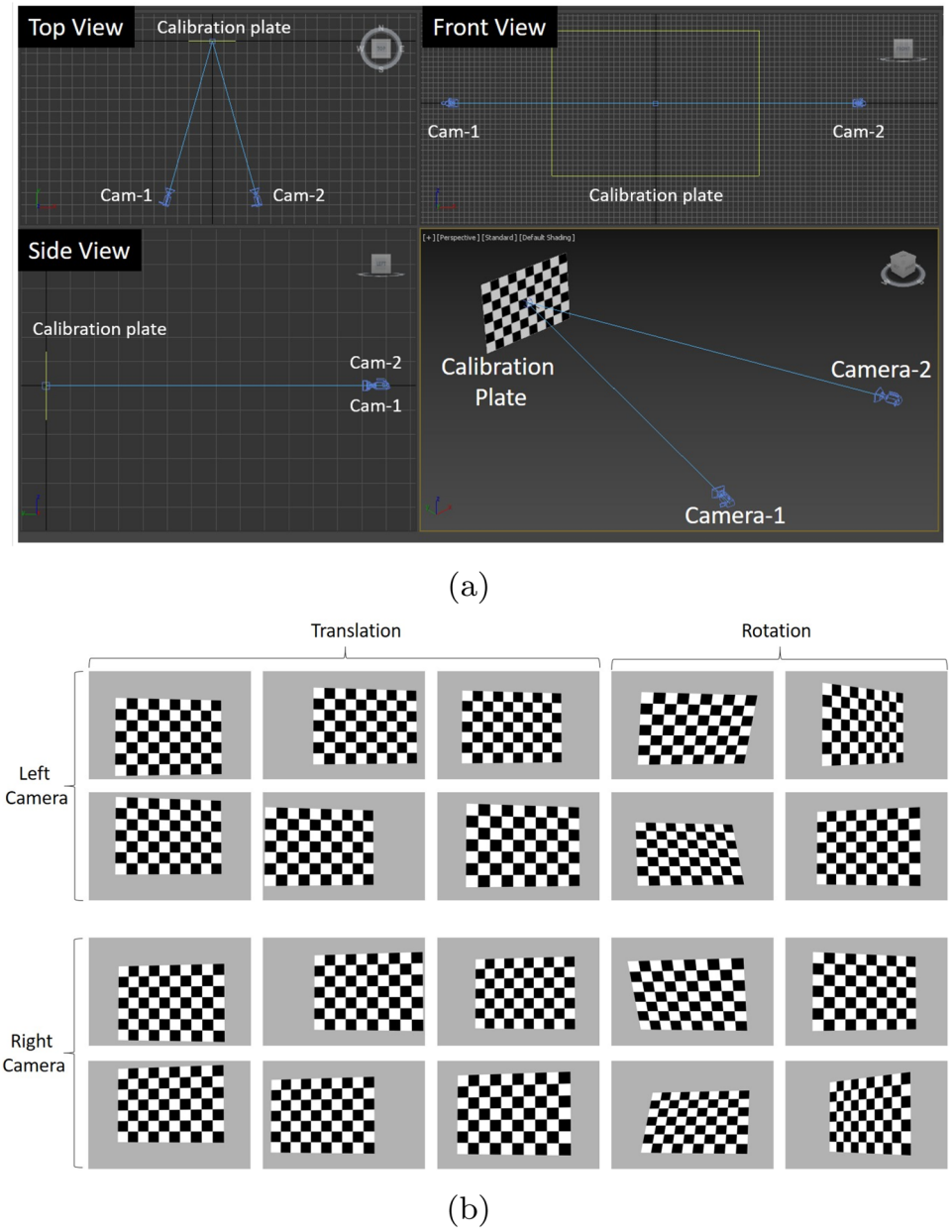

Fig. 5 Calibration setup in Autodesk 3ds Max **a** Virtual stereovision setup with calibration plate and the cameras, **b** Rendered images from camera-1 and camera-2 for calibration (selected)

was mounted with an arrangement that allows translations and rotations for the calibration purposes to avoid human involvement and unwanted deformations such as warping. The cameras were properly placed focusing on the board. The developed calibration setup makes the application of physical calibration method ideal to produce accurate parameters. At the same time, it can be used as model to design similar virtual stereovision system whose calibration parameters should match the ones obtained using physical approach. The IMU and laser sensors were used to measure the extrinsic parameters and also to place the cameras at desired position and orientation. The calibration images were captured in both of the cameras simultaneously for the calibration purpose. Using the extrinsic parameters from the extrinsic sensors and the camera parameters, the same virtual stereo system was designed in 3ds-MAX and the calibration images were rendered. Finally, the calibration process was carried out on the both sets of images and output parameters are compared. Basically, the calibration process that uses the images of physical calibration board is called the physical calibration method. On the other hand, the process using the virtually generated images is called virtual calibration method. The present study used the stereovision-combined calibration model for calibrating the stereo-DIC setups. In terms of calibration parameters, this calibration method provides intrinsic parameters of the cameras, i.e., principal points in X and Y axes (c_x, c_y) and focal length in X and Y axes (f_x, f_y), and the extrinsic parameters as the translations (t_x, t_y, t_z) and rotations (α, β, γ) of Camera 2 (right camera) with respect to Camera 1 (left camera). The α, β, γ are the rotation angles of Camera 2 about X, Y and Z axes of Camera 1. The rotation angles can be used to formulate the rotation matrix [R] to obtain the orientation of Camera 2 about Camera 1. Whereas, t_x, t_y, t_z are the translations of Camera 2 in X, Y and Z axes of Camera 1, which can be used to form the translation vector for the right-side camera, i.e., Camera 2. Table 1 shows the comparison between the physical calibration and virtual calibration methods on the basis of calibration parameters, it can be seen that the parameters are matching well. Also, the calibration errors (the average epipolar error and RMS error) for both the cases are well under the limit (maximum 0.5).

As the present study emphasizes the estimation of 3D vibration parameters, we used the developed novel calibration method for the indoor experiments carried out in previous study dealing with the vibration study of a pipe of 1m

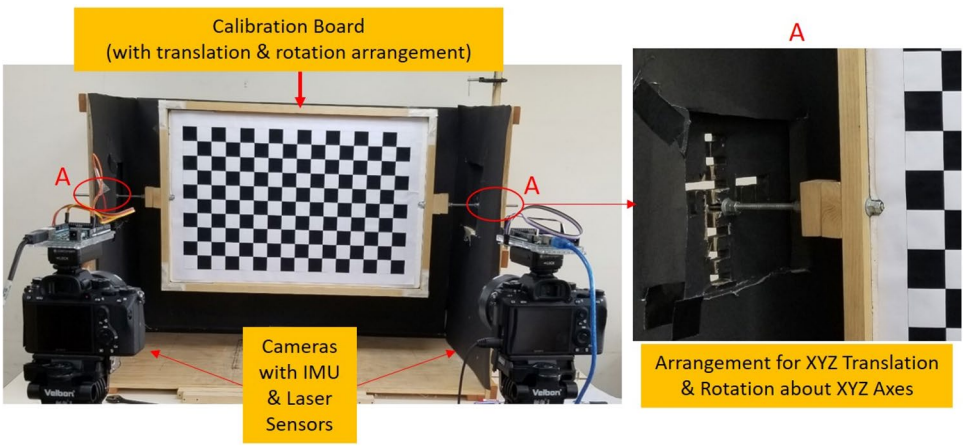

Fig. 6 Physical calibration setup for validation of the virtual stereovision assisted field stereo-DIC calibration method

Table 1 Comparison of stereo calibration parameters from physical and virtual calibration methods

Parameters	Physical calibration method		Virtual calibration method	
Intrinsic parameters	Camera 1	Camera 2	Camera 1	Camera 2
Principal Point, c_x (px)	621.9	668.6	630.5	643.8
Principal Point, c_y (px)	482.5	539.8	509.1	509.2
Focal Length, f_x (px)	5961.8	5788.7	6032.7	6087.3
Focal Length, f_y (px)	5943.9	577.1	6032.2	6086.8
Extrinsic parameters	Camera 2 w.r.t. Camera 1		Camera 2 w.r.t. Camera 1	
Translations (mm): t_x, t_y, t_z	-701.88, -26.6, -1.89		-712.4, -0.003, 110.5	
Rotations (rad): α, β, γ	0.001, 0.23, 0.006		0.00, 0.23, 0.00	
Calibration errors				
Avg. epipolar error	0.28		0.21	
RMS error	0.32		0.26	

height [29]. The pipe was excited using a hammer during the vibration test. The test setup and the results are shown in Fig. 7. It is important to note that the vibration results of the pipe are obtained by calibrating the DIC setup using physical calibration and virtual calibration methods. In the DIC setup, two Sony $\alpha 9$ cameras were used to design stereo camera setup and the images were recorded at 20 fps. It can be seen that displacements as well as the natural frequency are matching in both of the calibration cases. This validates that the virtual calibration method is helping the DIC setup generate accurate vibration results. The same can be expected in the case of larger structures. Here in the present study, we also studied the effect of varying frequency resolution, image resolution and the frame rate with the help of a high-speed DIC setup. The natural frequencies obtained using the calibration parameters from the virtual stereovision assisted calibration method are in excellent agreement with the ones calculated using physical calibration method (see Table 2). This comparison provides another validation and evidence for the suitability of using virtual calibration method for estimating vibrational parameters.

The developed novel calibration method is not only helpful in estimating the calibration parameters but also useful to design a desired multi-camera DIC systems (including stereo-DIC) for small-to-large scale applications. During our calibration experiments, we have observed that the application of IMU and laser sensors help in designing a desired 3D stereovision system. It is extremely useful to DIC field experiments for large structures. The positions and orientation of the cameras with respect to the desired region of interest (ROI) could be easily determined. They simplify the setup preparation which is often difficult with DIC experiments. In addition to that, this virtual stereovision assisted novel calibration method could also be used as a predictive-corrective calibration method to minimize calibration errors and obtain accurate results.

3 Application of the developed calibration method with DIC for field experiments

It has been established that we have developed and validated a potential calibration technique for calibrating stereovision or even multi-camera system for large structures applications. To demonstrate the capability of the the calibration technique, it was integrated with the DIC technique and used in two field experiments, one is based on a light tower and another deals with a utility-scale wind turbine. The final stereo-calibration-DIC methodology was basically used to find the 3D displacements and natural frequencies of the considered subjects/structures in the field.

3.1 Description and components of the complete methodology

Figure 8 describes the working procedures of developed methodology for calibration and application of stereo-DIC in the field applications. Components of the complete setup are given in Table 3. The procedure starts with the pre-designing of the stereovision system before performing the actual field experiment. With the known overall dimensions of the subject and camera specifications such as sensor size and focal length, it is possible to accurately determine the suitable positions and orientation of the cameras in the field. For the actual field experiment, construct the stereo-DIC setup by mounting the cameras on the tripods located at desired locations and connect the cameras with the triggering cable. We have used sturdy tripods to avoid the vibrations due to wind flowing over the cameras. Two Sony $\alpha 9$ cameras have been used to make the stereovision system. These are high-end digital cameras with decent frame rate capability of 20 fps with an image resolution of 6000px × 4000px. A customized remote controller is used for triggering the cameras simultaneously (an essential requirement for 3D-DIC analysis). Install the IMU sensor along with the Arduino microcontroller on the cameras to record their orientations. Place the laser sensor at appropriate location to obtain the positions of cameras with respect to the subject. Focus the cameras on the desired ROI on the subject. Then measure the extrinsic parameters of the designed field stereo-DIC setup using IMU and laser sensors, store these parameters for designing virtual stereovision system for calibration. Record the experiment images with appropriate aperture, shutter speed and ISO values and store them for performing correlation and vibration analysis. This finishes the field experiment part of the process. Now, for calibration, use the extrinsic parameters and cameras specifications to design the virtual stereovision system and then render the images of the virtual calibration plate at different positions and orientations. Supply the calibration images to the DIC software for calibration to obtain extrinsic and intrinsic parameters. The calibration accuracy can be ensured by changing the position and orientation of the calibration plate at the time of generating calibration images. More details on the developed calibration method are given in Fig. 3. To perform correlation and reconstruction, undistort the experiment images and supply them to the DIC software. Then, use the correlation values with calibration parameters to reconstruct the 3D displacement values in XYZ domain. It is important to note that the displacements of the structures were obtained in the Camera 1 (left camera) coordinate system. Digital Image Correlation Engine, also known as DICe, is used for calibration, correlation and reconstruction purposes. This open-source software is developed by researchers at Sandia National Laboratories (SNL) [43]. The natural frequencies are obtained by

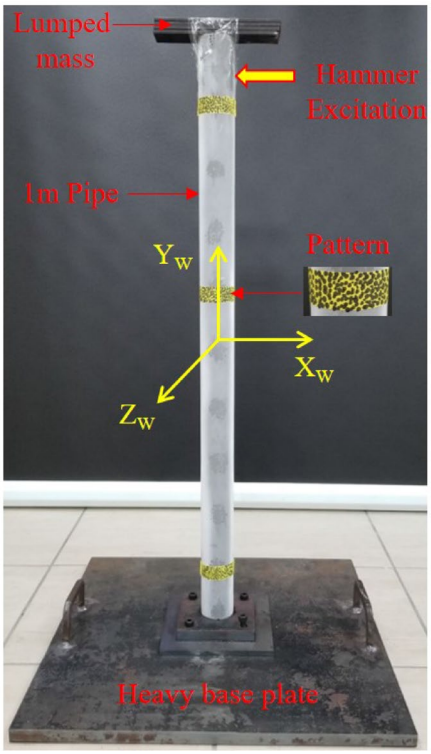
Lumped mass
Hammer Excitation
1m Pipe
Pattern
Y_w
X_w
Z_w
Heavy base plate

(a)

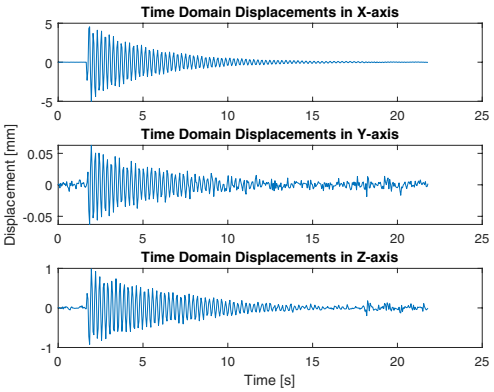
Time Domain Displacements in X-axis
Time Domain Displacements in Y-axis
Time Domain Displacements in Z-axis
Displacement [mm]
Time [s]

(b)

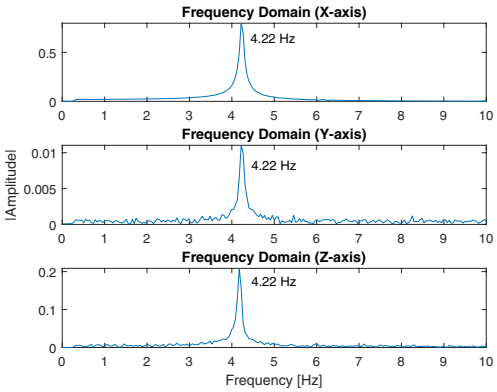
Frequency Domain (X-axis)
Frequency Domain (Y-axis)
Frequency Domain (Z-axis)
4.22 Hz
|Amplitude|
Frequency [Hz]

(c)

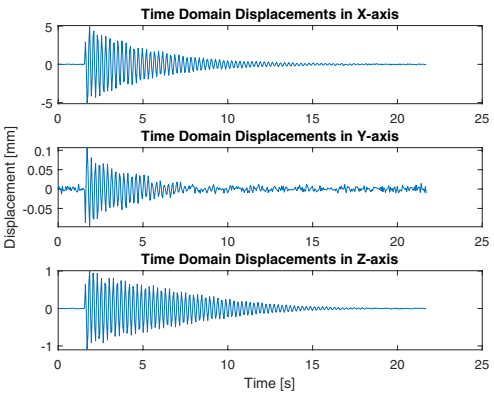
Time Domain Displacements in X-axis
Time Domain Displacements in Y-axis
Time Domain Displacements in Z-axis
Displacement [mm]
Time [s]

(d)

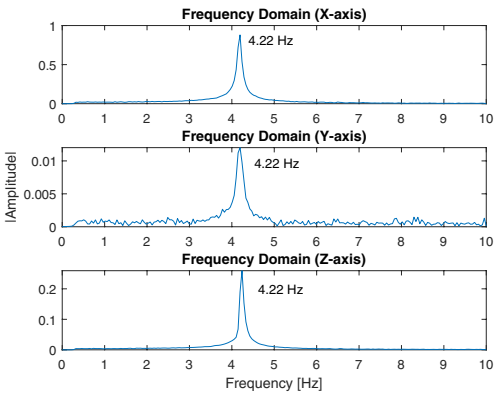
Frequency Domain (X-axis)
Frequency Domain (Y-axis)
Frequency Domain (Z-axis)
4.22 Hz
|Amplitude|
Frequency [Hz]

(e)

◂**Fig. 7** Comparison of virtual calibration and physical calibration methods in obtaining vibrational parameters, **a** Setup for vibration testing of the 1m pipe, **b** 3D displacements obtained using physical calibration, **c** Frequency response of the displacements obtained using physical calibration, **d** 3D displacements obtained using virtual calibration, **e** Frequency response of the displacements obtained using virtual calibration

performing FFT on the time-domain displacement values. A digital filter was designed in MATLAB to eliminate the impact of wind induced vibrations and noise due to correlation errors. The study uses high accuracy IMU and laser sensors to accurately measure the orientation and position of the cameras with respect to the selected ROIs on the structure. We have also used a triaxial accelerometer and a ground-based microwave interferometer for the purpose of validating the natural frequency values from the DIC technique.

3.2 Field Experiment-1: 10m light tower

The first field experiment was carried out on a light tower of 10 m height situated at a tennis court.

3.2.1 Experiment setup and stereo-calibration

As shown in the experimental setup in Fig. 9 and described during the development of the calibration method, the extrinsic parameters were obtained using the IMU-laser setup, which are used along with the cameras' specifications to design a virtual 3D-DIC setup in the Autodesk 3DS Max software. In this field experiment, the positions of the cameras with respect to each other and the light tower were measured using Laser Measure (GLM 50c Professional, Bosch). This laser sensor has a measurement range of 0.05-50.00 m with an accuracy of ±1.5 mm. The cameras were placed at a distance of 21.54m from the tower, whereas the distance between them was 9.09m. The FOV and ROI for the setup were found to be 9m × 6m and 470px × 3370px, respectively. The wired triggering was performed for simultaneous image recording. A triaxial accelerometer was used for the validation purpose. The natural frequencies obtained using DIC displacement data are compared with the ones obtained from the accelerometer. The complete experimental setup is shown in Fig. 9. In this experiment, we placed several artificial patterns for carrying out the measurement all over the tower. These patterns were created using white card board pieces of $200 \times 200mm^2$ size. Black dots were made using a thick black marker. The patterns were mounted using a silicon based double sided tape. The DIC experiment validating sensor i.e. the accelerometer, was mounted on the tower at the center. The accelerometer mounting was also done using silicon based double sided tape.

For the purpose of calibration, a checker-board based calibration plate of appropriate size (length 6m and breadth 4.2m) was designed in the virtual DIC system. Then, the calibration plate was rotated and translated while images were rendered at each step. The size of the rendered images, i.e. $6000px \times 4000px$, were kept same as exist for the used cameras. In total, 74 images were rendered using the virtual stereovision system that includes reference position and six positive and negative translations and rotations about each of all three axes. These images were supplied to the calibration tool in the DICe software for performing the calibration of the designed stereovision system for 10m light tower. Finally, the obtained calibration parameters, given in Table 6 in Appendix A, were provided to the image correlation program for the reconstruction purpose and obtain the vibrational parameters for the light tower.

Table 2 Comparison of virtual calibration and physical calibration methods in obtaining vibrational parameters, LS-DIC refers to low-speed DIC that uses the Sony $\alpha 9$ cameras (selected for the current study), whereas, HS-DIC refers to the high-speed camera DIC that uses Photron Mini UX50 cameras.

Method	Frame Rate (fps)	Image Resolution (px^2)	Frequency Resolution (Hz)	Natural Frequency (Hz)	
				Physical calibration method	Virtual calibration method
LS-DIC	20	6000 × 4000	0.046	4.22	4.22
	20	6000 × 4000	0.046	4.24	4.24
	60	1920 × 1080	0.008	4.22	4.22
	60	1920 × 1080	0.008	4.20	4.20
HS-DIC	50	1280 × 1024	0.009	4.24	4.24
	50	1280 × 1024	0.009	4.20	4.20
	500	1280 × 1024	0.024	4.24	4.24
	500	1280 × 1024	0.024	4.24	4.24
Coefficient of Variation (%)				0.37	0.37

Frequency resolution is the ratio of frame rate to the total number of images recorded

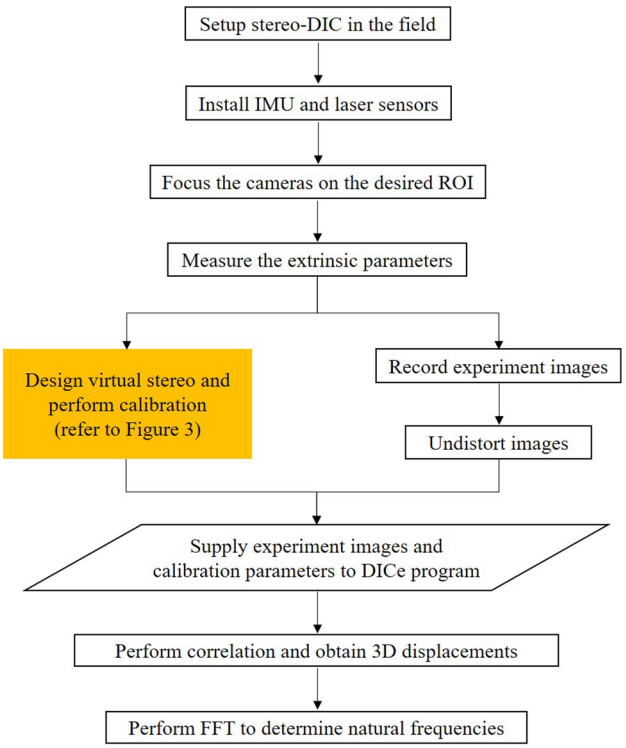

Fig. 8 A flowchart describing the calibration and application of stereo-DIC for large structures

3.2.2 Results and discussion

The displacements were obtained at three locations on the tower i.e. top, center and bottom. The excitation was carried out manually in the x-direction. Figure 10 shows the results for the manual pull-and-release excitation experiment. As the excitation is applied by pulling the tower slowly and the release, the tower seems to vibrate in a bending mode while having highest deflections at the top. This is evident from Figs. 10a, c and e showing displacements of top, center and bottom of the tower, respectively. The amplitude of deflections are larger in the x-direction, however, the tower has both in-plane and out-of-plane displacements. Due to these 3D vibrations, the natural frequencies are observed in all three directions at all the considered locations on the tower. For the purpose of validation, the results from accelerometer are presented in Fig. 11. It can be seen that the natural frequencies are matching closely. Hence, validates the 3D vibrations results from DIC.

As it is known that the large structures have low-frequency vibrations which are often difficult to investigate. Therefore, to estimate the consistency performance of the present DIC method, we have performed a comparison study on the basis of measuring the first fundamental mode. The comparison of DIC with accelerometer for various experimental configurations is shown in Table 4. It can be seen that the results from DIC are more consistent than accelerometer, even with different camera parameters and locations

Table 3 Details of the used hardware and software tools

Component	Model	Technical Specifications/Features
Digital Cameras (2)	Sony α9	Resolution (image): 6000 px × 4000 px
		Resolution (video): 1920 px × 1080 px
		Frame rate: 60 fps (video), 20 fps (image)
		Sensor Type: CMOS
		Lens Mount: E-mount
Optical Lens	Sony/SEL85F18	Focal Length:
		Maximum Aperture: F1.8
		Mount: E-mount
	Sony/SEL50M28	Focal Length:
		Maximum Aperture: F2.8 Macro
		Mount: E-mount
Accelerometer	PCB Piezotronics	Channels: Triaxial
		Frequency Range: 0.5 to 5000 Hz
		Measurement Range: ±50 g pk
DIC Software	DICe	Camera calibration, 2D and 3D DIC
DAQ Software	NI-LabVIEW	Data acquisition programming
DAQ Hardware	NI-9178, NI-9232	Data acquisition chassis and module
Accessories	Remote Controller, Sturdy Tripods, Flash Cards, Calibration Board	

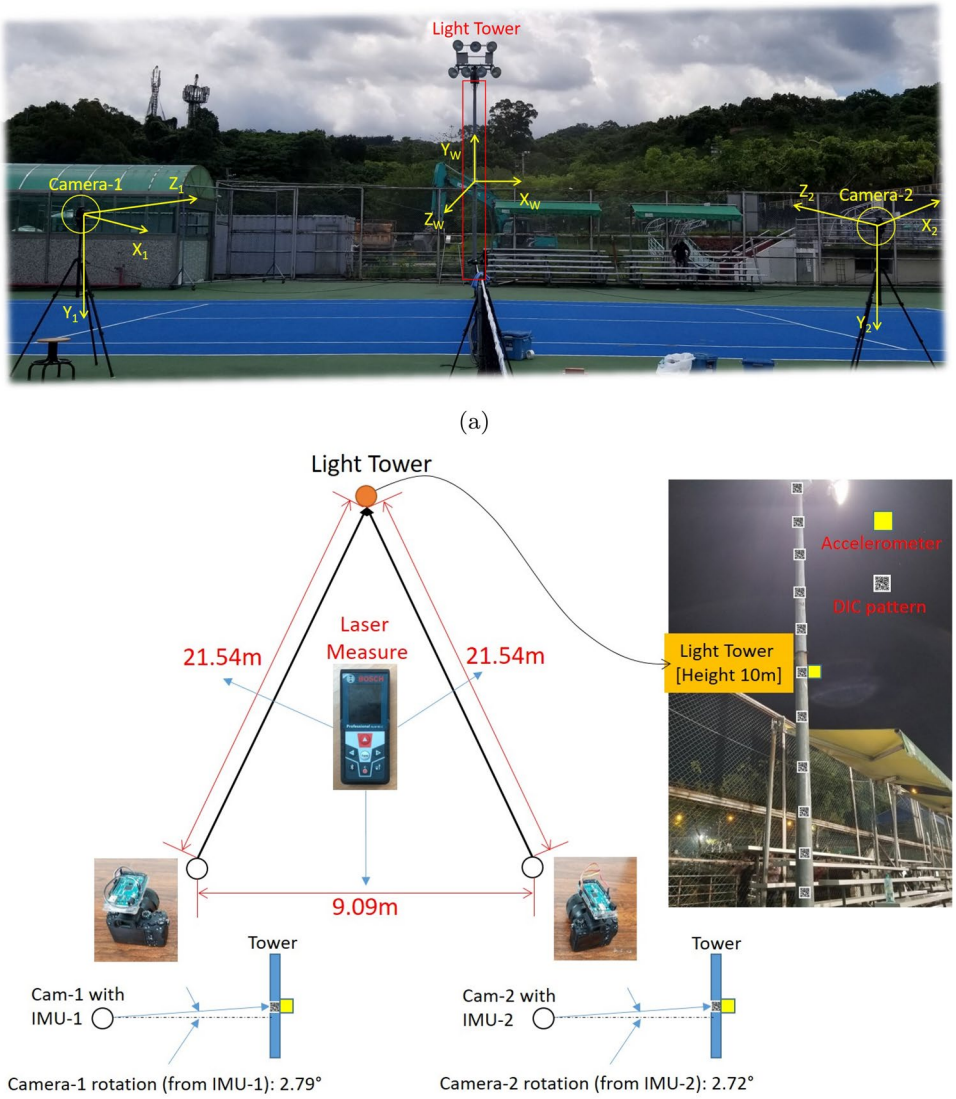

Fig. 9 3D-DIC setup for 10m light tower during Field Experiment 1

of pattern on the tower. It is directed that the DIC technique is superior for studying 3D vibrations of large-sized structures. On the top of that, displacement fields from DIC can be further analyzed for other studies including mode shapes derivation as well as qualitative and quantitative damage identification, localization and analysis, leading to extended health monitoring studies.

3.3 Field Experiment-2: Utility-scale wind turbine

The second field experiment was carried out with a utility-scale wind turbine of 2 MW capacity, 65 m tower height and 70 m rotor diameter.

3.3.1 Experimental setup and stereo-calibration

In this experiment, the measurement were carried out on the tower and one of the rotor blades. Therefore, two separate ROIs were chosen (one on the tower and second on the blade). The cameras were installed accordingly. Basically, two sets of experiments were carried out for the wind turbine case. Figure 12 shows the experimental setup consisting of cameras, IMU device, laser sensor, and the interferometer. Figure 13 shows the selected regions of interest as well as the identified natural patterns. A natural pattern has been identified at the top of the tower to measure its natural frequencies. While, three patterns are located on the blade along its span that could be useful to perform extended modal analysis. For the purpose of calibrating this system, the IMU-Arduino device is used to measure orientation

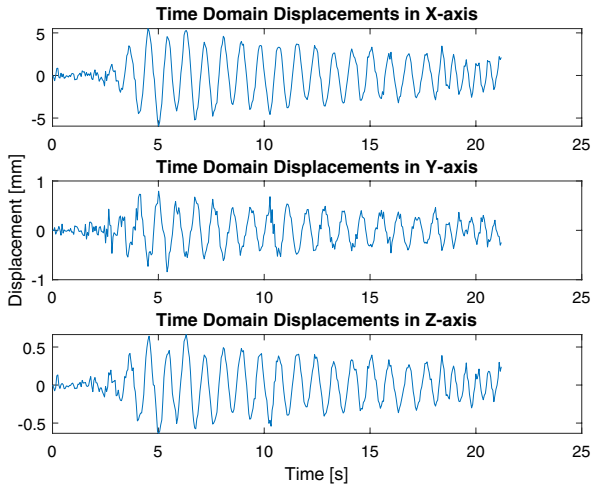
Time Domain Displacements in X-axis
Time Domain Displacements in Y-axis
Time Domain Displacements in Z-axis
Displacement [mm]
Time [s]

(a)

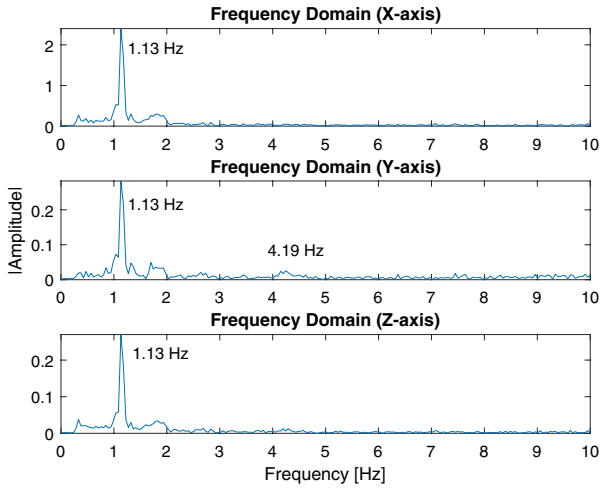
Frequency Domain (X-axis)
Frequency Domain (Y-axis)
Frequency Domain (Z-axis)
1.13 Hz
4.19 Hz
|Amplitude|
Frequency [Hz]

(b)

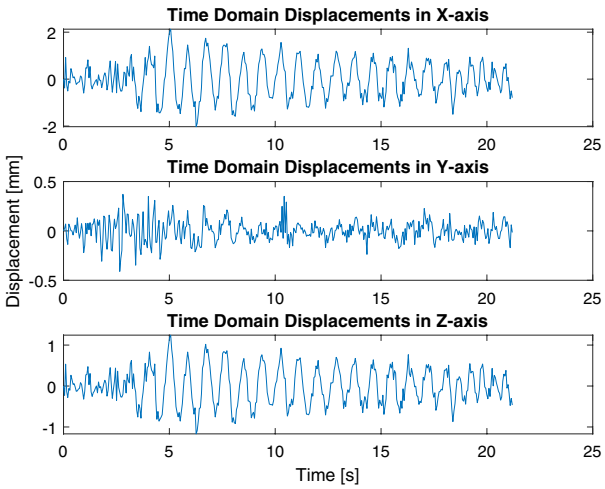
Time Domain Displacements in X-axis
Time Domain Displacements in Y-axis
Time Domain Displacements in Z-axis
Displacement [mm]
Time [s]

(c)

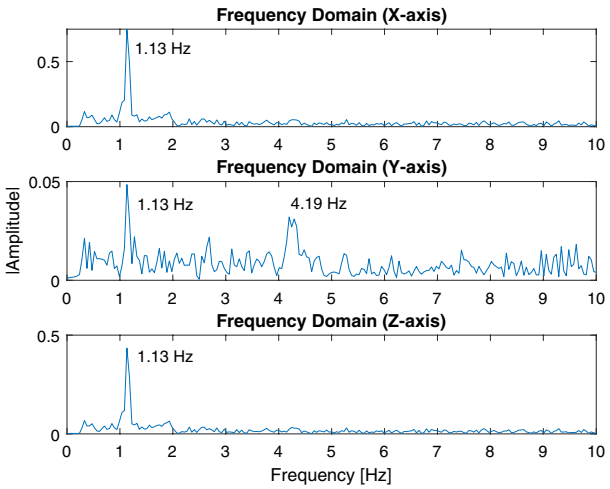
Frequency Domain (X-axis)
Frequency Domain (Y-axis)
Frequency Domain (Z-axis)
1.13 Hz
4.19 Hz
|Amplitude|
Frequency [Hz]

(d)

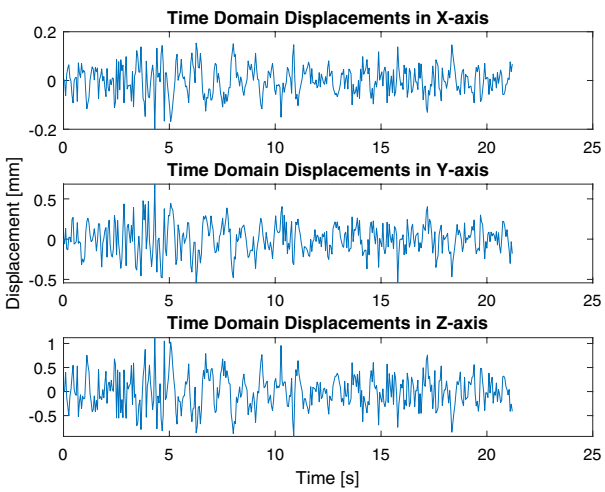
Time Domain Displacements in X-axis
Time Domain Displacements in Y-axis
Time Domain Displacements in Z-axis
Displacement [mm]
Time [s]

(e)

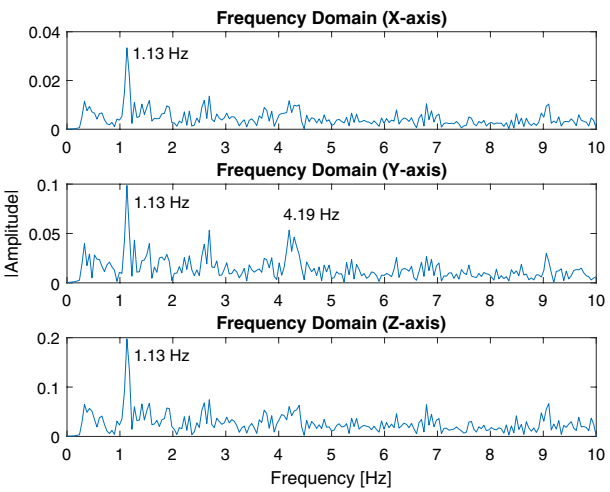
Frequency Domain (X-axis)
Frequency Domain (Y-axis)
Frequency Domain (Z-axis)
1.13 Hz
4.19 Hz
|Amplitude|
Frequency [Hz]

(f)

◂**Fig. 10** DIC results for 10m light tower with manual pull-and-release excitation case, **a** 3D displacements of the pattern at the top, **b** natural frequencies from the displacements of the pattern at the top, **c** 3D displacements of the pattern at the center, **d** natural frequencies from the displacements of the pattern at the center, **e** 3D displacements of the pattern at the bottom, **f** natural frequencies from the displacements of the pattern at the bottom

angles of the cameras. In this field experiment, Nikon N2 Total Station is used to measure the coordinates of the cameras and reference points in the selected ROIs. The sensor provides long distance measurement range of up to 3000m with an accuracy of 2mm + 2ppm. The virtual stereovision in Autodesk 3DS Max is designed using measured distances and the rotation angles. The checker-board based calibration plate of $60 \times 42\ m^2$ size is designed and rotated-translated to generate calibration images (total 74 images including reference position with translations and rotations about XYZ axes). These images are supplied to the calibration tool in the DIC program for performing calibration. Finally, the obtained calibration parameters, given in Table 7 in Appendix A, are provided to the image correlation program for the reconstruction purpose. The obtained natural frequency results have been compared with the results from ground-based microwave interferometer for the validation purpose.

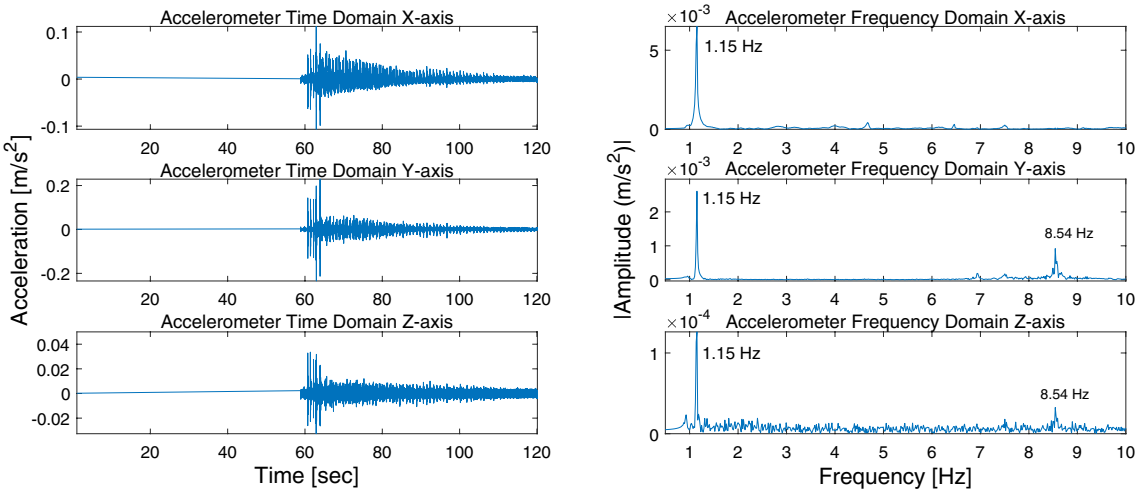

(a) (b)

Fig. 11 Accelerometer results for 10m light tower with manual excitation, **a** three axes acceleration measured at the center, **b** natural frequencies from the acceleration values at the center

Table 4 Comparison of DIC with the accelerometer on the basis of consistency in measurement

Excitation Mode	Camera parameters			First mode frequency [Hz]	
	Exposure time	ISO speed	F-stop	3D-DIC	Accelerometer
Wind	1/250 sec	ISO-250	f/10	1.14	1.14
Manual	1/250 sec	ISO-250	f/10	1.13	1.15
Wind	1/500 sec	ISO-125	f/10	1.13	1.15
Manual	1/500 sec	ISO-125	f/10	1.13	1.14
Manual	1/500 sec	ISO-250	f/10	1.14	1.15
Manual	1/500 sec	ISO-500	f/10	1.15	1.15
Manual	1/500 sec	ISO-1000	f/10	1.14	1.16
Wind	1/250 sec	ISO-125	f/10	1.15	1.16
Manual	1/250 sec	ISO-125	f/10	1.14	1.15
Manual	1/250 sec	ISO-500	f/10	1.14	1.15
Manual	1/500 sec	ISO-125	f/4	1.14	1.16
Manual	1/250 sec	ISO-50	f/4	1.14	1.15
Average of fundamental natural frequency				1.14	1.15
Coefficient of Variation, %				0.49	0.64

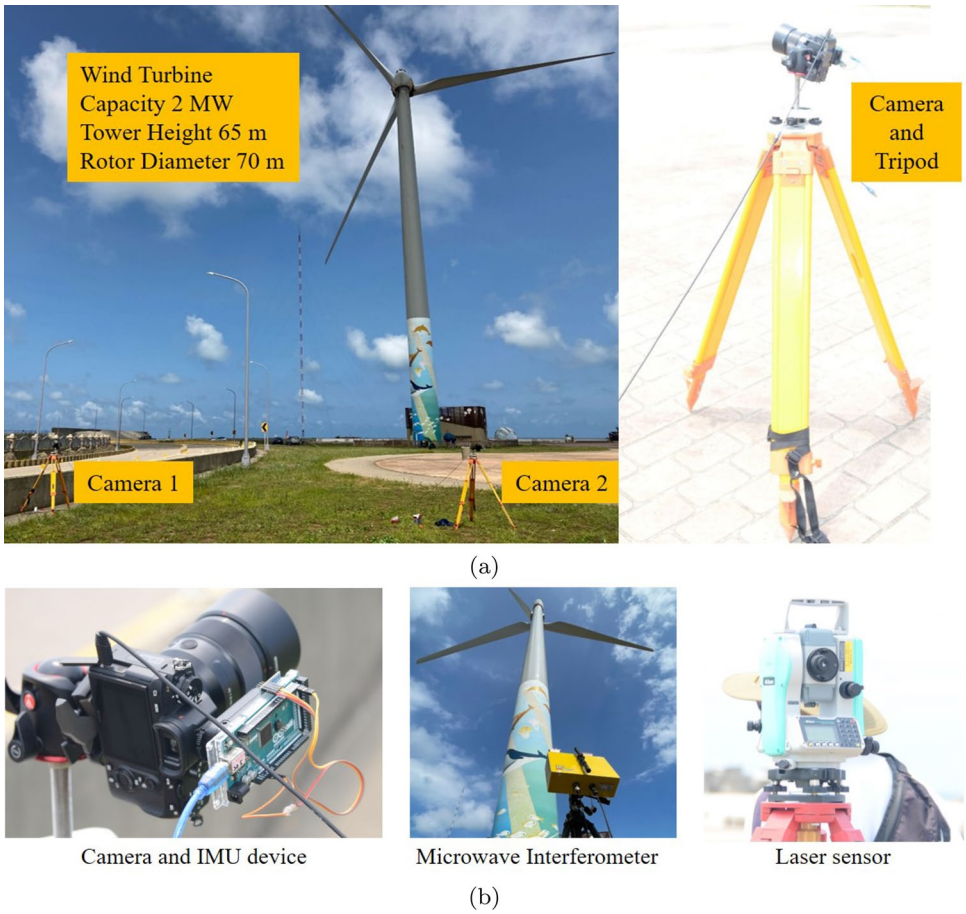

Fig. 12 Field experiment setup for wind turbine, **a** Cameras and the wind turbine, **b** Cameras with other sensors. The positions of the Camera 1 and Camera 2 with respect to the center of the FOV are 57.31m and 57.93m, respectively. The tilt angles of the Camera 1 Camera 2 focusing on the center of the FOV are 36.09° and 38.09°, respectively

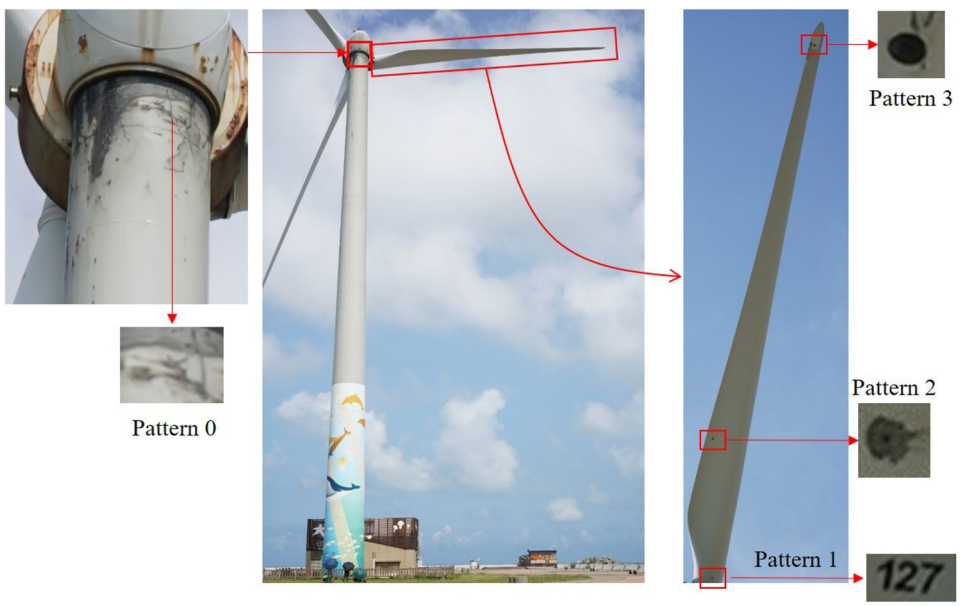

Fig. 13 Wind turbine and the natural patterns

3.3.2 Results and discussion

Figure 14 shows the results for the tower of the wind turbine. The displacements were obtained for the natural pattern (Pattern 0) identified near the nacelle of the wind turbine. It can be seen that the 3D displacements as well as natural frequencies are successfully measured. The first fundamental natural frequency of the tower is 0.42 Hz that is close to 0.44

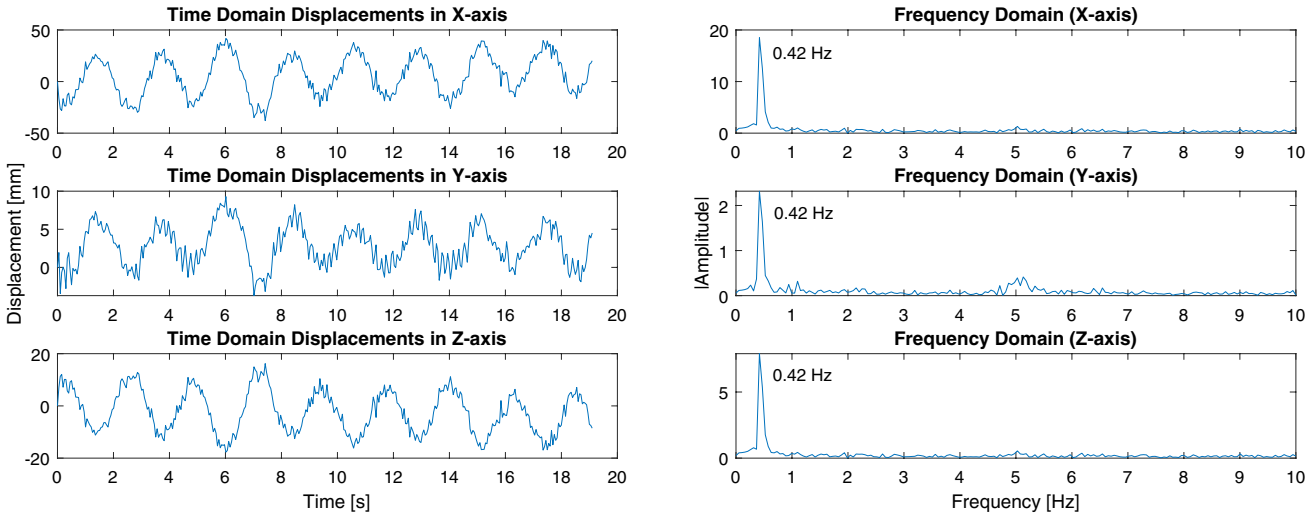

Fig. 14 DIC results for the tower of the wind turbine, **a** displacements and **b** natural frequencies obtained using a natural pattern (Pattern 0) present at the top of the tower

Hz measured using microwave interferometer. In the present study, the interferometer technique was applied only on the tower of the turbine. The results for the three patterns on the blade are shown in Fig. 15. There are seven modes that have been identified from the blade. These include the first fundamental mode of the tower, i.e., 0.42 Hz. As pattern 1 is near the base of the long-span blade, unlike other patterns, it shows the lower frequency fundamental mode, i.e., 1.2 Hz (apart from 0.42 Hz of the tower). The amplitude of displacements is increasing along the span (Pattern 1–3) for each of the axes indicating that the blade is vibrating in the bending mode. It should also be noted that the DIC method is able to obtain the natural frequencies approximately up to 10 Hz. This could be due to significantly higher amplitude of the displacements (because of high flexibility) of the blade as compared to the tower.

All the natural frequencies obtained in the present study are compared with the results using microwave interferometer. In another study [44], the interferometer technique was used extensively to perform vibration study of wind turbines. In that study, the technique was applied to the tower as well as the blades of multiple turbines. Table 5 shows the comparison of DIC and interferometer techniques on the basis of natural frequencies. Based on the comparison, it can be said that the methods agree with each others for lower frequency modes. However, the other modes occurred at different frequencies but they are in similar range. It should be noted that the results from the interferometer were obtained in the past for wind turbines of the same model investigated in the current study. The characteristics of the blades are expected to be somewhat different in terms of mass and structural configurations. The rotor blade is a slender structure. It is quite susceptible to the environmental conditions. Considering the obtained results, it can be concluded that the developed DIC-calibration methodology is sensitive enough to identify various natural frequency modes of the order of up to 10 Hz. The method also provides 3D displacements that are useful to perform extended modal analysis of large structures.

4 Conclusions

The present study establishes a novel stereo camera calibration method for performing digital image correlation (DIC) measurements on large structures. The calibration approach adopts IMU and laser sensors for extrinsic parameters and a virtual stereovision model for intrinsic parameters. The developed novel calibration technique is successfully implemented in the field experiments by calibrating the stereo-DIC setup for 10m light tower and a 65m wind turbine. It is observed that the combined DIC-calibration methodology is able to determine 3D displacements and natural frequencies of the structures. The errors in the measurement of extrinsic parameters on the vibration results were insignificant due to high accuracy of the sensors. The IMU and Total Station devices provide the values of orientations and positions of the cameras with the accuracy of $\pm 0.1^\circ$ and ± 2mm, respectively. The proposed calibration method has also been effective in selecting optimal parameters for field experiments such as size of field of view (FOV), the stereo angle and baseline (distance between the cameras).

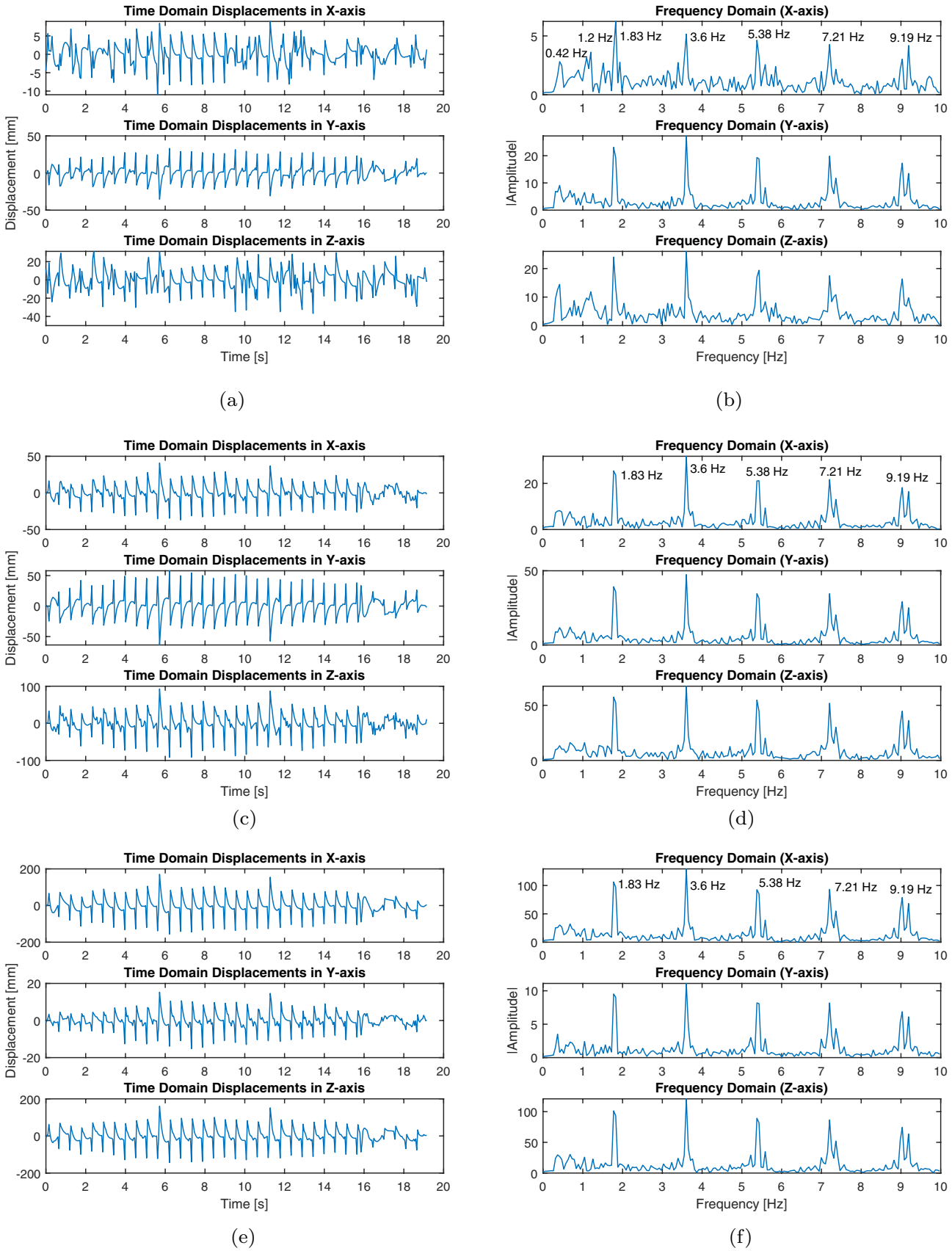

Fig. 15 DIC results for the blade of the wind turbine, **a**, **b** displacements and natural frequency for Pattern 1, **c**, **d** displacements and natural frequency for Pattern 2, **e**, **f** displacements and natural frequency for Pattern 3

Table 5 Comparison between DIC and microwave interferometer

Technique	Natural Frequencies (Hz)						
	Mode 1	Mode 2	Mode 3	Mode 4	Mode 5	Mode 6	Mode 7
3D-DIC	0.42	1.2	1.83	3.6	5.38	7.21	9.19
Interferometer	0.44	1.12	2.9	3.48	3.78	4.22	9.06

The light tower experiments helped in establishing the applicability the developed DIC-calibration methodology for large structures. The experiment was also used as a platform to verify the consistency of the method in the measurement of natural frequencies. In the case of wind turbine experiments, the developed methodology showed its importance by identifying various vibration modes up to 10 Hz. The results are found to be accurate for lower frequency modes by comparing them with those obtained using the microwave interferometer. Furthermore, the measured 3D displacements of the wind turbine tower and blade would be useful to generate mode shapes of such large structures provided that potential natural patterns are available. The present study could be considered as the base for tracking multiple points on large structures. With that, an extended structural dynamic characterization of bridges and wind turbines would become an economical and non-contact alternative to other approaches using contact-type sensor arrays.

Based on the present work, it can be said that the developed DIC-based non-contact technique with the proposed novel calibration method is effective to perform 3D vibration testing of various large-sized civil and aerospace structures. However, the methodology can be further improved by developing in-house DIC programs that could automatically identify and correlate natural patterns. In the same direction, the use of virtual stereo software could be replaced by a mathematical model that would not only generate the calibration images but also perform the calibration. This would simplify the calibration process and provide the scope for additional improvements. The application of 3D-DIC technique in the field experiments has potential to become a better alternative to 2D displacement measurements using microwave interferometer and other techniques. The vibration analysis and damage assessment of large civil structures will be more efficient in the near future as the proposed technique improves in aspects including the automatic identification and correlations of natural patterns.

Appendix A Calibration parameters for field experiments

See Table 6.

Table 6 Stereo calibration parameters for field experiment on 10m light tower. The α, β, γ are the rotation angles of Camera 2 (Cam2) about X, Y and Z of axes of Camera 1 (Cam1). Whereas, t_x, t_y, t_z are the translations of Camera 2 (Cam2) in X, Y and Z of axes of Camera 1 (Cam1)

Intrinsic Parameters			Extrinsic Parameters	
Parameters	Cam1	Cam2	Parameters	Cam1 to Cam2
Principal Point c_x (px)	3023.91	3001.34	Translations (mm): t_x, t_y, t_z	-8906.29, 93.76, 1934.65
Principal Point c_y (px)	1992.15	1964.93	Rotations (rad): α, β, γ	-0.003, 0.426, -0.023
Focal Length f_x (px)	14396.21	8266.57		
Focal Length f_y (px)	14393.43	8275.23		

Table 7 Stereo calibration parameters for field experiment on the wind turbine. The α, β, γ are the rotation angles of Camera 2 (Cam2) about X, Y and Z of axes of Camera 1 (Cam1). Whereas, t_x, t_y, t_z are the translations of Camera 2 (Cam2) in X, Y and Z of axes of Camera 1 (Cam1)

Intrinsic Parameters			Extrinsic Parameters	
Parameters	Cam1	Cam2	Parameters	Cam1 to Cam2
Principal Point c_x (px)	3001.35	3002.89	Translations (mm): t_x, t_y, t_z	-9455.4, 1.26, 1379.48
Principal Point c_y (px)	1998.93	1998.65	Rotations (rad): α, β, γ	0.00, 0.16, 0.00
Focal Length f_x (px)	11467.52	11464.45		
Focal Length f_y (px)	11469.28	11465.65		

Acknowledgements This research was made possible by the support from the Ministry of Science and Technology, Taiwan through project number MOST 108-2221-E-324. Support was also received from the research grants of the Chaoyang University of Technology. The authors would like to thank Dr. Jiunnren Lai for his support through numerous times of discussion. We appreciate very much the sound advices from Professor Yishuo Huang and the technical assistance of Mr. Jia-Jian Honh. Thanks are also due to Mr. Po-Chun Cheng, Mr. Chin-Hao Tseng, Mr. Alok Kumar Sharma, Mr. Bineri, and Dr. Edwin M Lau for their extended support during field experiments.

Declarations

Conflict of interest The authors declare that they have no conflict of interest.

References

1. Xu Y, Brownjohn JM (2018) Review of machine-vision based methodologies for displacement measurement in civil structures. J Civil Struct Health Monit 8(1):91–110
2. Baqersad J, Poozesh P, Niezrecki C, Avitabile P (2017) Photogrammetry and optical methods in structural dynamics — a review. Mech Syst Signal Process 86:17–34
3. Niezrecki C, Baqersad J, Sabato A (2018) Digital image correlation techniques for NDE and SHM. In: Ida N, Meyendorf N (eds), Handbook of Advanced Non-Destructive Evaluation, Springer, Cham, Ch. 43, pp 1545–1590
4. Lin Y-C, Chiang C-H, Yu C-P, Hsu K-T (2020) Deterministic deterioration modeling of wind turbines toward the failure identification - a modal curvature approach. J Struct Integr Maint 5(2):104–112
5. Brownjohn JM, De Stefano A, Xu Y-L, Wenzel H, Aktan AE (2011) Vibration-based monitoring of civil infrastructure: challenges and successes. J Civil Struct Health Monit 1(3–4):79–95
6. Kudus SA, Sugiura K, Suzuki Y, Matsumura M (2019) Dynamic response measurement of steel plate structure utilising video camera method. J Civil Struct Health Monit 9(5):597–605
7. Clemente P, Bongiovanni G, Buffarini G, Saitta F (2019) Structural health status assessment of a cable-stayed bridge by means of experimental vibration analysis. J Civil Struct Health Monit 9(5):655–669
8. Pan B, Qian K, Xie H, Asundi A (2009) Two-dimensional digital image correlation for in-plane displacement and strain measurement: a review. Meas Sci Technol 20(6):062001
9. Pan B (2018) Digital image correlation for surface deformation measurement: historical developments, recent advances and future goals. Meas Sci Technol 29(8):082001
10. Peters WH, Ranson WF (1982) Digital imaging techniques in experimental stress analysis. Opt Eng 21(3):427–431
11. Sutton MA, Wolters WJ, Peters WH, Ranson WF, McNeill SR (1983) Determination of displacements using an improved digital correlation method. Image Vis Comput 1(3):133–139
12. Luo PF, Chao YJ, Sutton MA, Peters WH (1993) Accurate measurement of three-dimensional deformations in deformable and rigid bodies using computer vision. Exp Mech 33(2):123–132
13. Silva LC, Petraglia MR, Petraglia A (2004) A robust method for camera calibration and 3-D reconstruction for stereo vision systems. In: IEEE European Signal Processing Conference, Vienna, Austria,
14. Orteu J-J (2009) 3-D computer vision in experimental mechanics. Opt Lasers Eng 47(3):282–291
15. Reu P (2012) Introduction to digital image correlation: best practices and applications. Exp Tech 36(1):3–4
16. Stinville J, Francis T, Polonsky A, Torbet C, Charpagne M, Chen Z, Balbus G, Bourdin F, Valle V, Callahan P, et al (2020) Time-resolved digital image correlation in the scanning electron microscope for analysis of time-dependent mechanisms. Exp Mech 1–18
17. Kumar D, Kamle S, Mohite P, Kamath G (2019) A novel real-time DIC-FPGA-based measurement method for dynamic testing of light and flexible structures. Meas Sci Technol 30(4):045903
18. Chiang C-H, Shih M-H, Chen W, Yu C-P (2011) Displacement measurements of highway bridges using digital image correlation methods. In: Seventh International Symposium on Precision Engineering Measurements and Instrumentation, Vol. 8321, International Society for Optics and Photonics, p 83211G
19. Pan B, Tian L, Song X (2016) Real-time, non-contact and targetless measurement of vertical deflection of bridges using off-axis digital image correlation. NDT & E Int 79:73–80
20. Feng Y, Dai F, Zhu H-H (2015) Evaluation of feature- and pixel-based methods for deflection measurements in temporary structure monitoring. J Civil Struct Health Monit 5(5):615–628
21. Xiao P, Wu Z, Christenson R, Lobo-Aguilar S (2020) Development of video analytics with template matching methods for using camera as sensor and application to highway bridge structural health monitoring. J Civil Struct Health Monit 1–20
22. Feng D, Feng MQ, Ozer E, Fukuda Y (2015) A vision-based sensor for noncontact structural displacement measurement. Sensors 15(7):16557–16575
23. Kim S-W, Kim N-S (2013) Dynamic characteristics of suspension bridge hanger cables using digital image processing. NDT & E Int 59:25–33
24. Wang Y, Brownjohn J, Capilla JAJ, Dai K, Lu W, Koo KY (2021) Vibration investigation for telecom structures with smartphone camera: case studies. J Civil Struct Health Monit 11(3):757–766
25. Brown N, Schumacher T, Vicente MA (2021) Evaluation of a novel video- and laser-based displacement sensor prototype for civil infrastructure applications. J Civil Struct Health Monit 11(2):265–281
26. Baqersad J, Carr J, Lundstrom T, Niezrecki C, Avitabile P, Slattery M (2012) Dynamic characteristics of a wind turbine blade using 3D digital image correlation. In: Health Monitoring of Structural and Biological Systems 2012, Vol. 8348, International Society for Optics and Photonics, p 83482I
27. Nonis C, Niezrecki C, Yu T-Y, Ahmed S, Su C-F, Schmidt T (2013) Structural health monitoring of bridges using digital image correlation. In: Health Monitoring of Structural and Biological Systems 2013, Vol. 8695, International Society for Optics and Photonics, p 869507
28. Poozesh P, Baqersad J, Niezrecki C, Avitabile P, Harvey E, Yarala R (2017) Large-area photogrammetry based testing of wind turbine blades. Mech Syst Signal Process 86:98–115
29. Kumar D, Chiang C-H, Lin Y-C, Hsu K-T (2020) 3D vibration studies of large rotating structures using DIC. In: Health Monitoring of Structural and Biological Systems IX, Vol. 11381, International Society for Optics and Photonics, p 1138124
30. Sabato A, Reddy N, Khan S, Niezrecki C (2018) A novel camera localization system for extending three-dimensional digital image correlation. In: Nondestructive Characterization and Monitoring of Advanced Materials, Aerospace, Civil Infrastructure, and Transportation XII, Vol. 10599, International Society for Optics and Photonics, p 105990Y
31. Sabato A, Niezrecki C (2019) Development of an IMU-radar sensor board for three-dimensional digital image correlation camera triangulation. In: Health Monitoring of Structural and Biological Systems XIII, Vol. 10972, International Society for Optics and Photonics, p 109721V

32. Sabato A, Valente NA, Niezrecki C (2020) Development of a camera localization system for three-dimensional digital image correlation camera triangulation. IEEE Sens J 20(19):11518–11526
33. Reagan D, Sabato A, Niezrecki C (2018) Feasibility of using digital image correlation for unmanned aerial vehicle structural health monitoring of bridges. Struct Health Monit 17(5):1056–1072
34. Khadka A, Fick B, Afshar A, Tavakoli M, Baqersad J (2020) Non-contact vibration monitoring of rotating wind turbines using a semi-autonomous UAV. Mech Syst Signal Process 138:106446
35. Reagan D, Sabato A, Niezrecki C (2017) Unmanned aerial vehicle acquisition of three-dimensional digital image correlation measurements for structural health monitoring of bridges. In: Nondestructive Characterization and Monitoring of Advanced Materials, Aerospace, and Civil Infrastructure 2017, Vol. 10169, International Society for Optics and Photonics, p 1016909
36. Dorafshan S, Maguire M (2018) Bridge inspection: human performance, unmanned aerial systems and automation. J Civil Struct Health Monit 8(3):443–476
37. Kumar D, Chiang C-H, Lin Y-C (2021) Identification and correlation of natural patterns using a hybrid BRISK-DIC method. In: Nondestructive characterization and monitoring of advanced materials, aerospace, civil infrastructure, and transportation XV, vol. 11592. International Society for Optics and Photonics, p 115920K
38. Sutton MA, Orteu J-J, Schreier H (2009) Image correlation for shape, motion and deformation measurements: basic concepts, theory and applications. Springer Science & Business Media
39. Sutton MA, McNeill SR, Helm JD, Chao YJ (2000) Advances in two-dimensional and three-dimensional computer vision. In: Rastogi PK (ed) Photomechanics. Springer, Berlin, pp 323–372
40. Koohbor B, Mallon S, Kidane A, Sutton MA (2014) A DIC-based study of in-plane mechanical response and fracture of orthotropic carbon fiber reinforced composite. Compos B Eng 66:388–399
41. Sutton MA, Yan JH, Tiwari V, Schreier H, Orteu J-J (2008) The effect of out-of-plane motion on 2D and 3D digital image correlation measurements. Opt Lasers Eng 46(10):746–757
42. Pan B, Yu L, Wu D, Tang L (2013) Systematic errors in two-dimensional digital image correlation due to lens distortion. Opt Lasers Eng 51(2):140–147
43. Turner D (2015) Digital Image Correlation Engine (DICe) Reference Manual, Sandia Report, SAND2015-10606 O. Tech. rep, Sandia National Laboratories
44. Chiang C-H, Hsu K-T, Yu C-P, Cheng C-C, Pan J-Z (2018) Remote measurements and vibration analysis of existing wind turbines. J Test Eval 47(3):2193–2206